Supplemental information

Supplemental Figures and legends

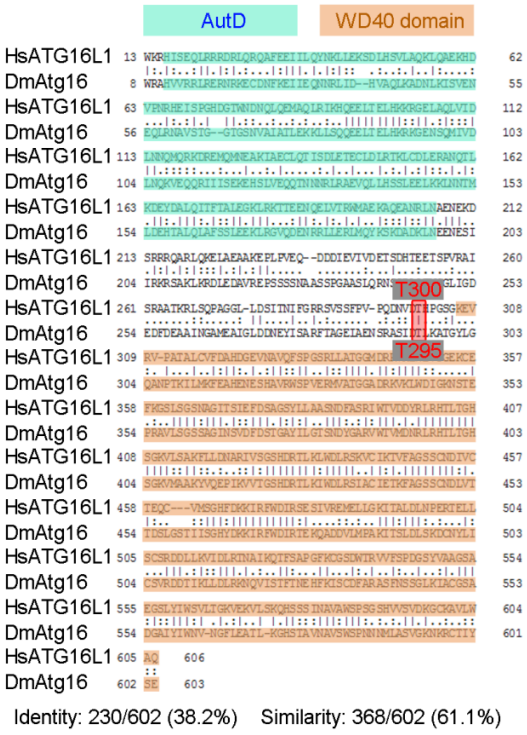

Fig. S1: Protein sequence alignment of human Atg16L1 and *Drosophila* Atg16. Identical protein regions and the position of human T300 and fly T295 are highlighted, based on homology between human Atg16L1 and fly Atg16 isoform C (the only Atg16 isoform that is expressed in the intestine, see Fig. S2A).

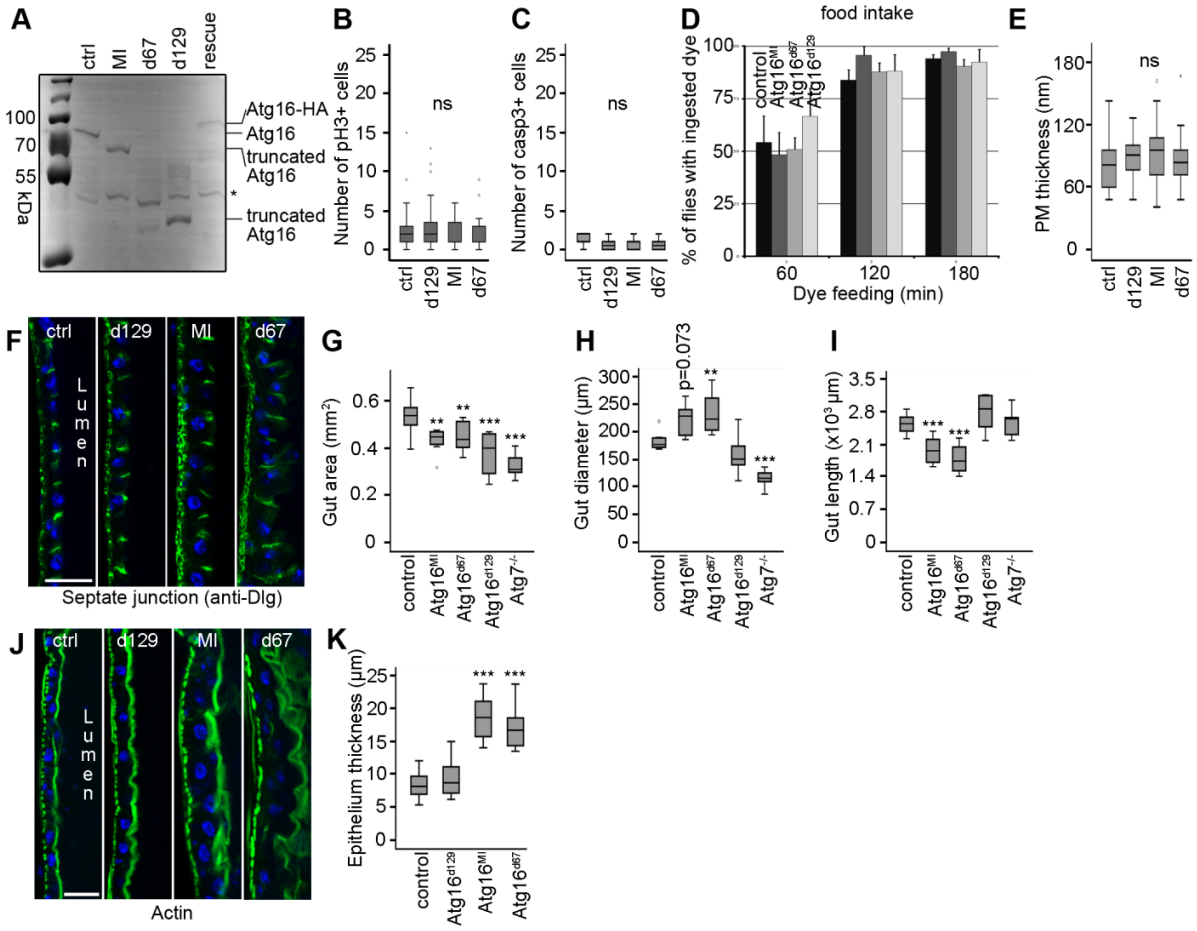

Fig. S2: Gut architecture and physiology is altered in Atg16 WD40 mutants. (A) Atg16 expression in gut protein extracts from different mutants and genetically rescued flies. Asterisk marks a non-specific band that serves as loading control. (B, C) The number of mitotic (B, N=8-9) and active caspase-3 positive apoptotic (C, N=5-6) cells does not change in 5-day-old control and *Atg16* mutant guts, Kruskal-Wallis tests. (D) Time course analysis of flies with ingested blue dye-containing food reveals no difference in feeding activity in the indicated *Atg16* mutants and controls. N=115-120, ANOVA. (E) Quantification of peritrophic membrane (PM) thickness from ultrastructural images. N=3, ANOVA. (F) Distribution and number of septate junctions marked by anti-Dlg appears similar in controls and different *Atg16* mutant intestinal walls. (G-I) Measurements of gut area (G, N=7-10, ANOVA), diameter (H, N=7-12, ANOVA) and length (I, N=7-13, ANOVA) in controls and *Atg16* mutants. (J) Anti-Actin staining shows the thickening of the gut epithelium in $Atg16^{MI}$ and $Atg16^{d67}$ mutant intestines compared

to control and *Atg16*^{d129} mutants, quantified in K. N=15, ANOVA. ** and *** represent p<0.05 and p<0.001 in G, H, I, K, respectively. Bars: 20 µm (F, J).

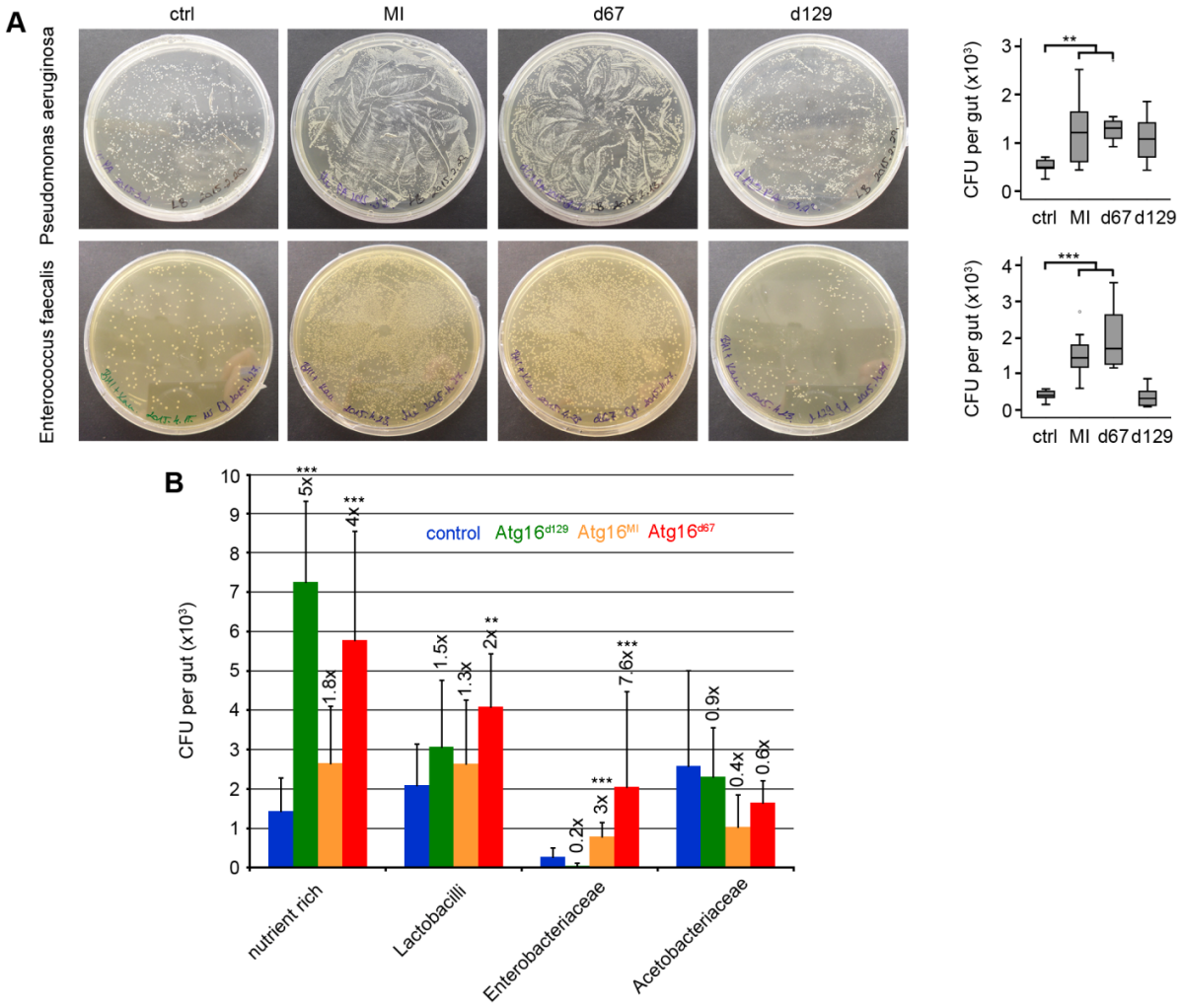

Fig. S3: Intestinal bacteria numbers change in *Atg16* mutant guts. (A) Representative images of bacteria derived from isolated and plated single guts following PA (N=10, ANOVA) and EF (N=9-10, ANOVA) oral infections. (B) Differential alterations in intestinal microbiota in various *Atg16* mutants. Numbers indicate fold change compared to the control in colony forming units (CFUs). N=7-11, ANOVA. ** and *** represent $p<0.05$ and $p<0.001$ in A, B, respectively.

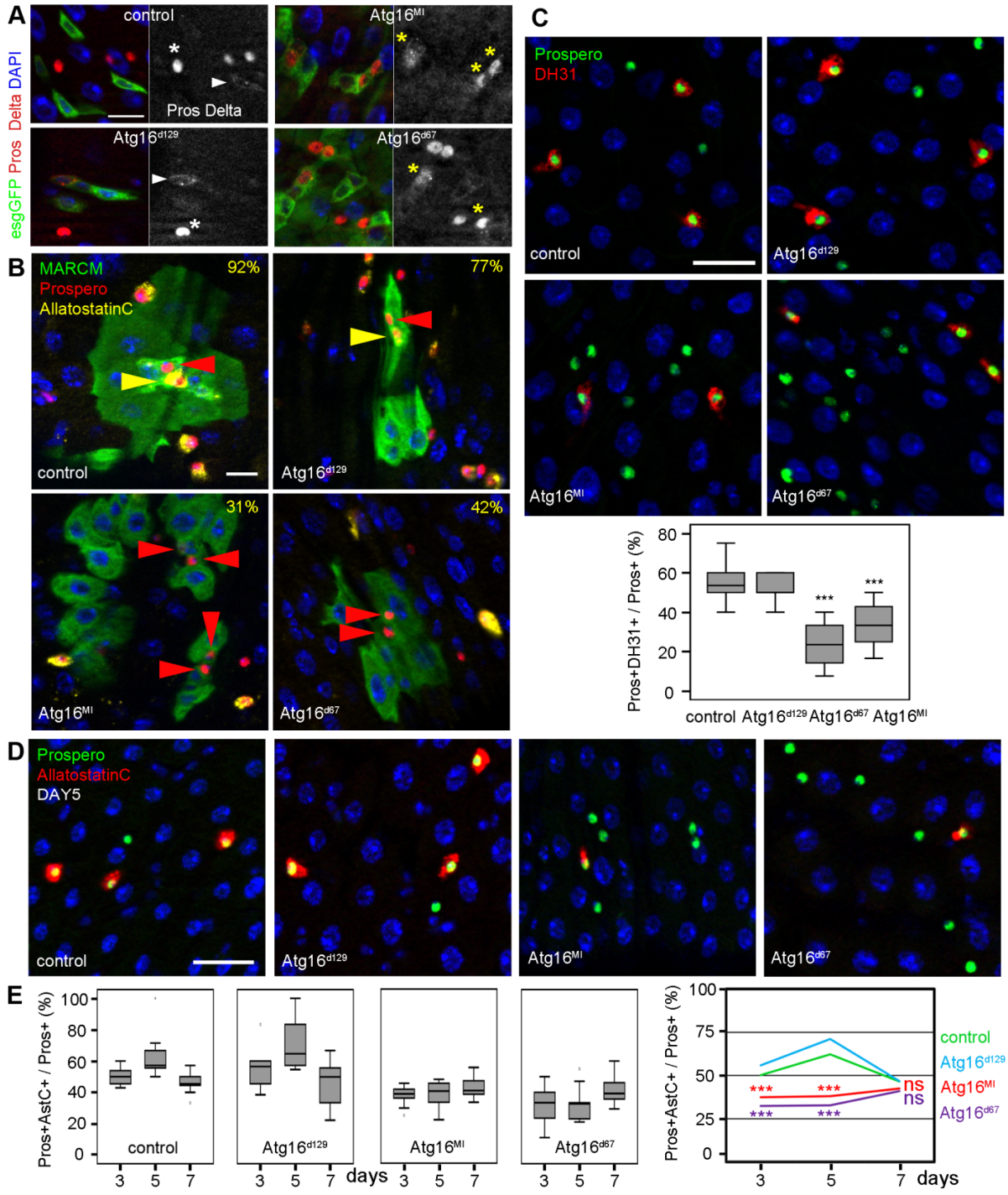

Fig. S4: Regulatory peptide expression in *Atg16* mutant guts. (A) Prospero and Delta co-label esgGFP+ pre-EEs in *Atg16*^{MI} and *Atg16*^{d67} mutant intestines. Arrowheads point to esgGFP+ Delta+ ISCs, white and yellow asterisks mark esgGFP+ Prospero+ and esgGFP+ Delta+ Prospero+ EE and preEE cells, respectively. (B) AllatostatinC (AstC) expression in different *Atg16* mutant clones. Yellow arrowheads indicate AstC-

producing Prospero+ mature EE cells, and red arrowheads point to Prospero+ cells that show no AstC expression. % refers to the average ratio of Pros+ AstC+ / all Pros+ cells within clones in the different genotypes, indicating a decrease of mature EEs in *Atg16*^{Ml} and *Atg16*^{d67} mutant clones. (C) The ratio of DH31-producing Prospero+ cells declines in *Atg16*^{Ml} and *Atg16*^{d67} mutant guts compared to controls, while it does not change in *Atg16*^{d129} mutants. N=10, ***: $p<0.001$, ANOVA. (D) Fewer AstC-producing Prospero+ cells are seen in *Atg16*^{Ml} and *Atg16*^{d67} mutant guts compared to controls, while it does not change in *Atg16*^{d129} mutants. (E) Time course analysis of the ratio of AstC-producing Prospero+ mature EE cells reveals a delay in EE differentiation in *Atg16*^{Ml} and *Atg16*^{d67} mutant guts compared to controls, while it does not change in *Atg16*^{d129} mutants. N=5, ***: $p<0.001$, ANOVA. Bars: 20 μm (A, C, D), 10 μm (B).

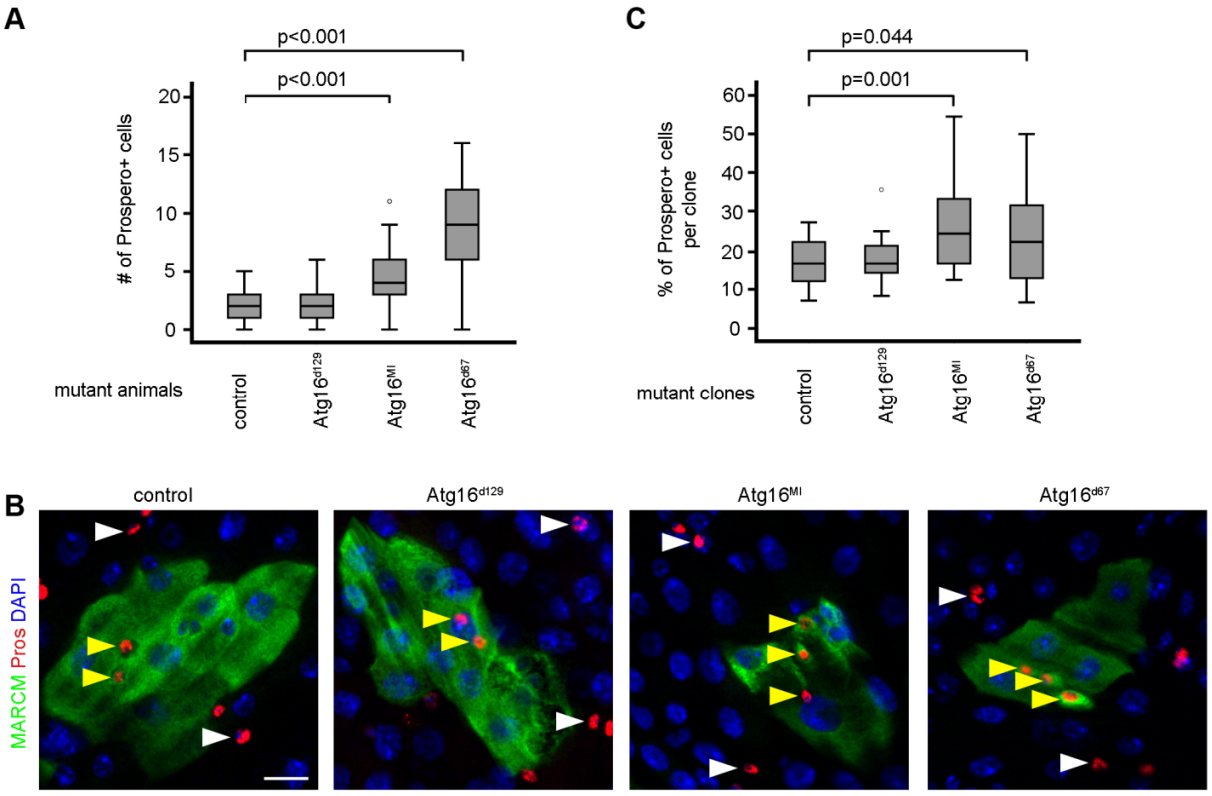

Fig. S5: Atg16 promotes EE differentiation. (A) Quantification of all Prospero-positive cells in *Atg16* mutants that are shown in Fig. 2C-F. N=6-12, Kruskal-Wallis test. (B) Prospero-positive (pre)-EE cell numbers increase in *Atg16^{MI}* and *Atg16^{d67}* mutant clones in mosaic intestines, as the percentage of Prospero+ cells in GFP-marked cell clones is higher than in control clones. Yellow arrowheads show Prospero-positive cells within the clones, white arrowheads indicate such cells outside of the clones. (C) Quantification of data. N=10, ANOVA. Bar: 20 µm (B).

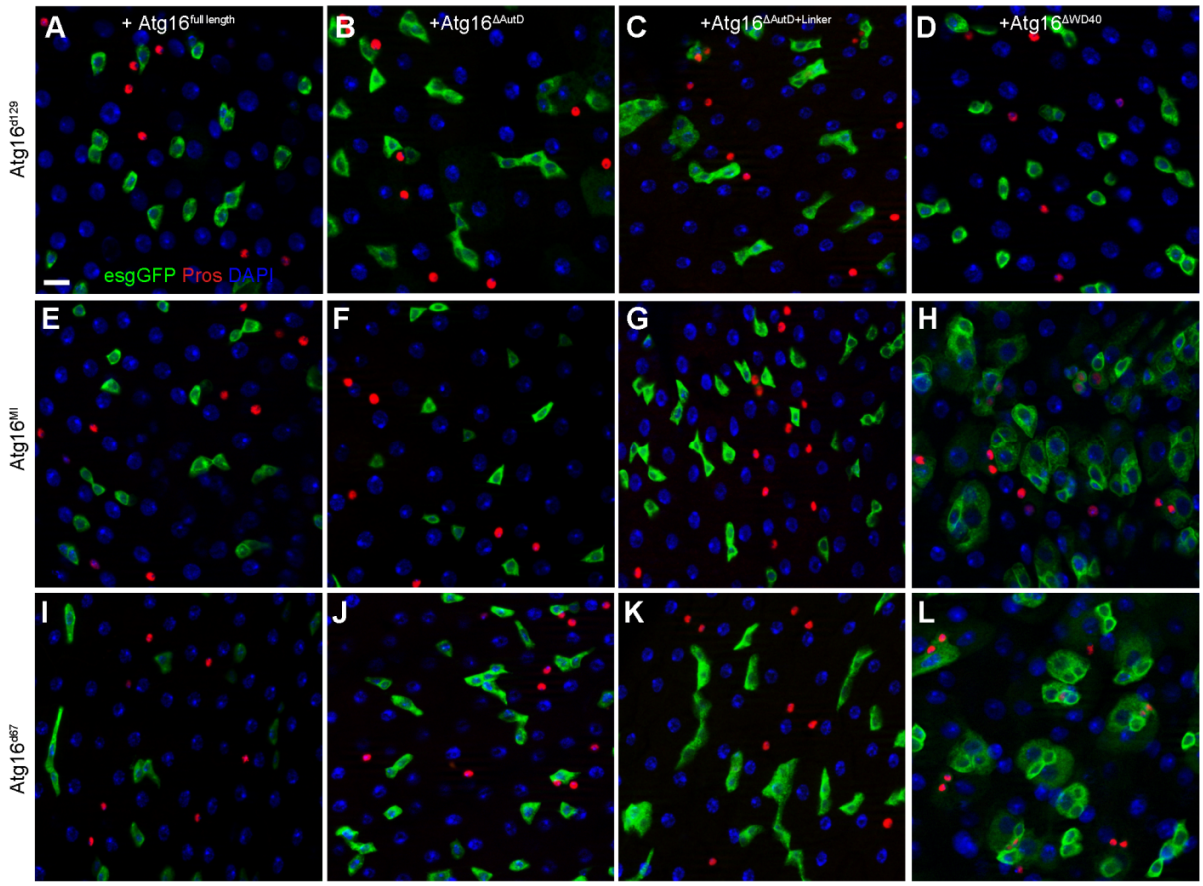

Fig. S6: Atg16 WD40 domain restores EE differentiation in WD40 mutants. Esg-specific overexpression of Atg16$^{\text{full length}}$ (E, I), Atg16$^{\Delta AutD}$ (F, J) and Atg16$^{\Delta AutD+Linker}$ (G, K) rescues the EE cell differentiation defect of *Atg16^{MI}* and *Atg16^{d67}* mutant intestines, while these genetic manipulations have no effect on EE cells in the *Atg16^{d129}* mutant (A-D). Esg-specific overexpression Atg16$^{\Delta WD40}$ does not affect EE differentiation status in *Atg16* mutants (D, H, L). See Fig. 2G for quantification of data. Bar: 10 µm (A-L).

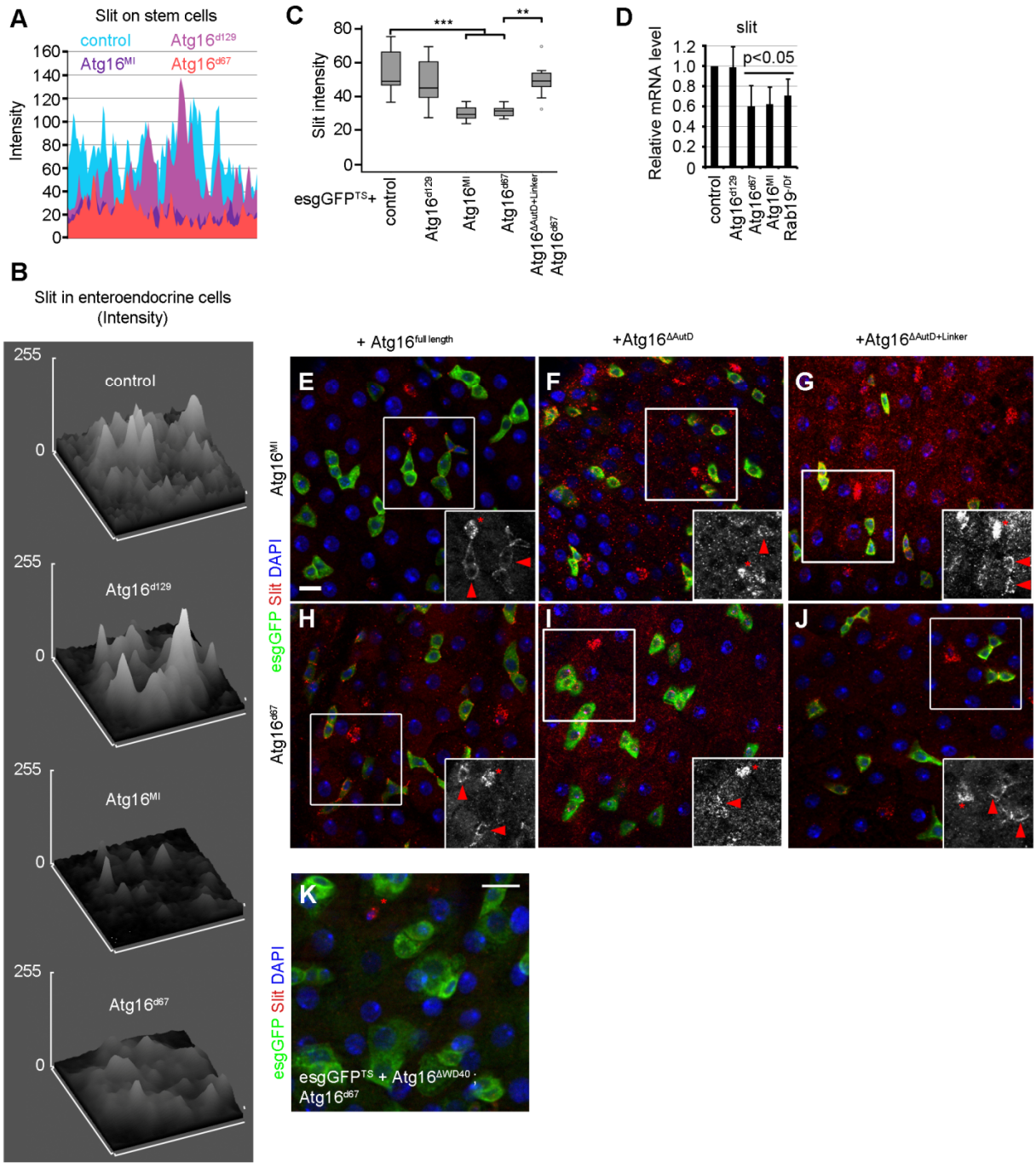

Fig. S7: Atg16 WD40 domain promotes Slit/Robo signaling. (A) Histogram shows overall Slit intensity on intestinal stem cells in wild type and different *Atg16* mutants. (B) Surface plot profiles of Slit intensity in Prospero-positive cells of wild-type and *Atg16* mutants. (C) Slit staining intensity decreases in $Atg16^{MI}$ and $Atg16^{d67}$ intestines, which is fully restored by WD40 domain ($Atg16^{\Delta AutD+Linker}$) overexpression in $Atg16^{d67}$ mutants.

N=10, ***: p<0.001, **: p<0.01, ANOVA. (D) Slit mRNA expression decreases in *Atg16*^{MI}, *Atg16*^{d67} and *Rab19* mutant intestines compared to controls, whereas it does not change in *Atg16*^{d129} mutant guts. (E-J) Esg-specific overexpression of Atg16$^{\text{full length}}$ (E and H), Atg16$^{\Delta\text{AutD}}$ (F and I) and Atg16$^{\Delta\text{AutD+Linker}}$ (G and J) restores Slit production in EE cells and Slit localization on stem cells in *Atg16*^{MI} (E-G) and *Atg16*^{d67} (H-J) mutant intestines, respectively. (K) Escargot-specific overexpression of Atg16$^{\Delta\text{WD40}}$ does not restore Slit production in *Atg16*^{d67} mutants. Red asterisks indicate Slit-producing EE cells in E-K, while red arrowheads show Slit localization on stem cells in E-J. Bar: 10 μm (E-J), 20 μm (K).

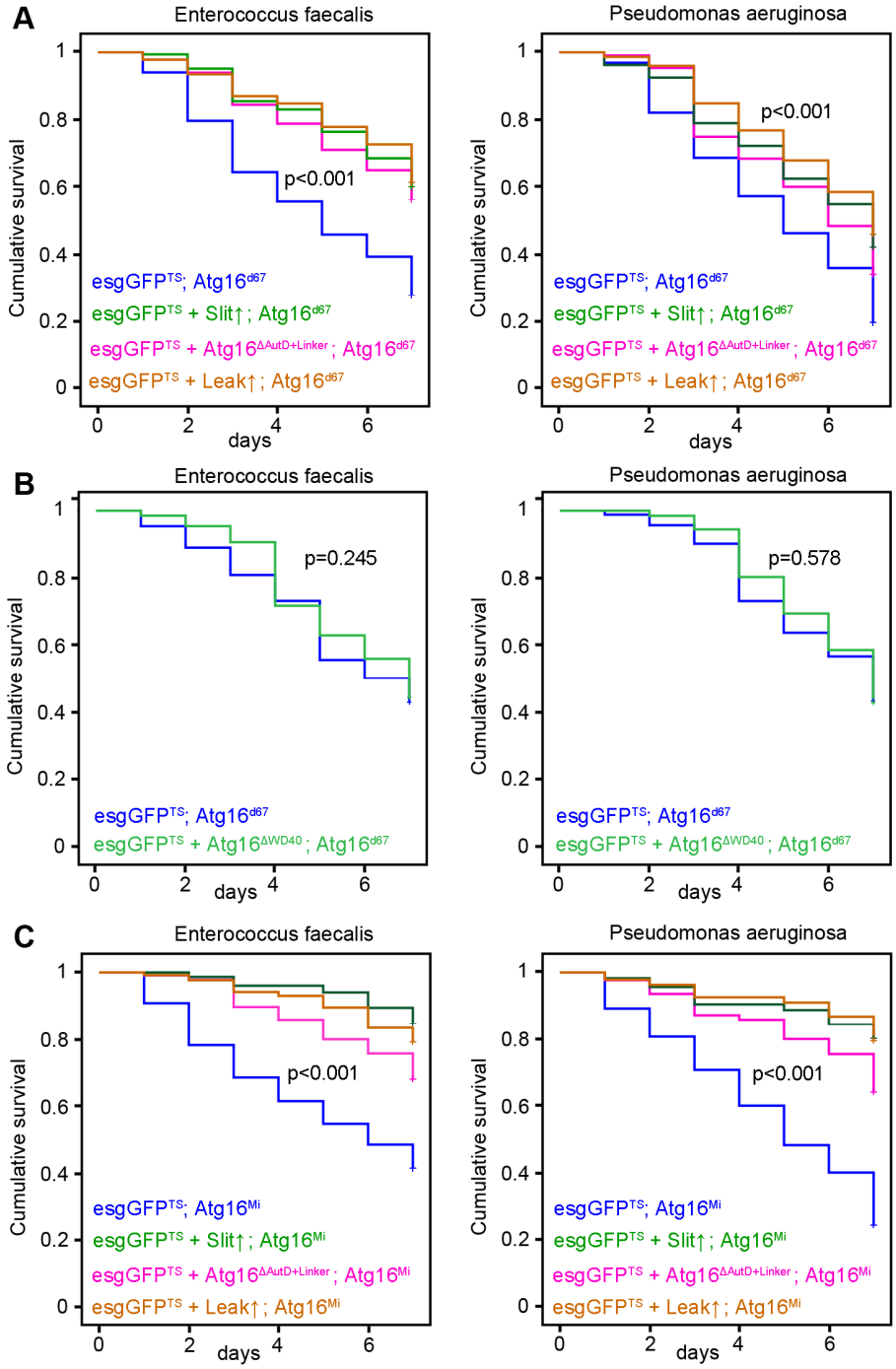

Fig. S8: Slit, Robo2 and Atg16 WD40 domain overexpression improves the resistance of WD40 mutants to bacterial infection. (A, C) Esg-specific overexpression of Slit, Atg16 WD40 domain ($Atg16^{\Delta AutD+Linker}$) and Leak/Robo2 increases resistance to oral bacterial infection with EF and PA in *Atg16*^{d67} (A) and *Atg16*^{Ml} (C) mutant flies. Kaplan-Meier survival curves are shown, p-values are

calculated by Log-rank analyses. (B) Esg-specific overexpression of Atg16$^{\Delta WD40}$ in *Atg16^{d67}* mutants does not improve resistance to oral infection by PA or EF. Kaplan-Meier survival curves are shown, and p-values were calculated by Log-rank analyses. N=166-344 (EF) and N=133-290 (PA) for panel A, N=395-509 (EF) and N=424-508 (PA) for panel B, N=152-339 (EF) and N=116-280 (PA) for panel C.

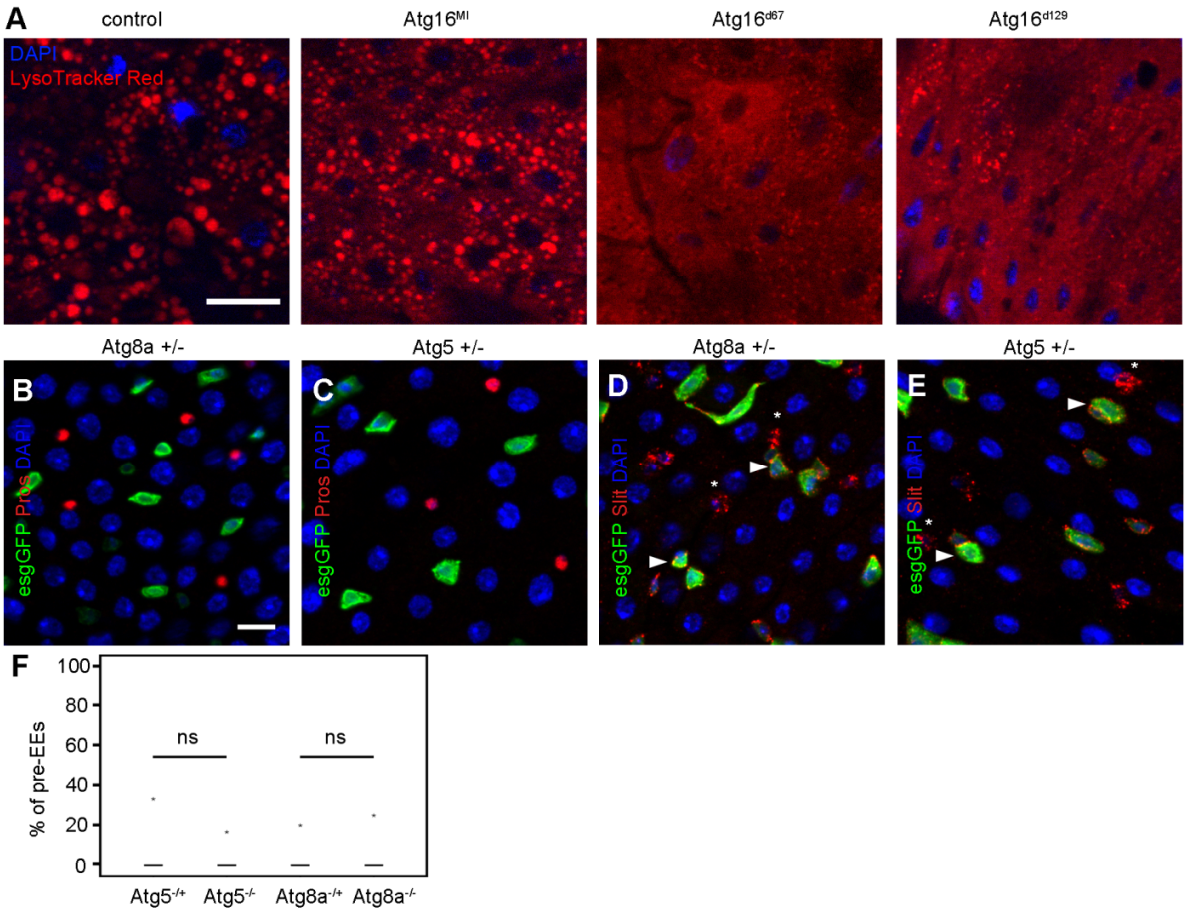

Fig. S9: Autophagy in *Atg16* mutants and EE differentiation in *Atg5* and *Atg8a* heterozygotes. (A) Acidic compartments labeled by LysoTracker Red decrease in *Atg16*^{d129} and *Atg16*^{d67} autophagy mutant midguts compared to control and *Atg16*^{MI} mutant animals. (B-E) *Atg8a* and *Atg5* heterozygous midguts do not show any cell differentiation or Slit localization defects. (F) Quantification of Prospero+ esgGFP+ / total Prospero+ cell data from panels B, C (genotype controls) and Fig. 6K, L (homozygous *Atg8a* and *Atg5* mutants). N=5, two-tailed two-sample T tests. Bar: 20 µm (A), 10 µm (B).

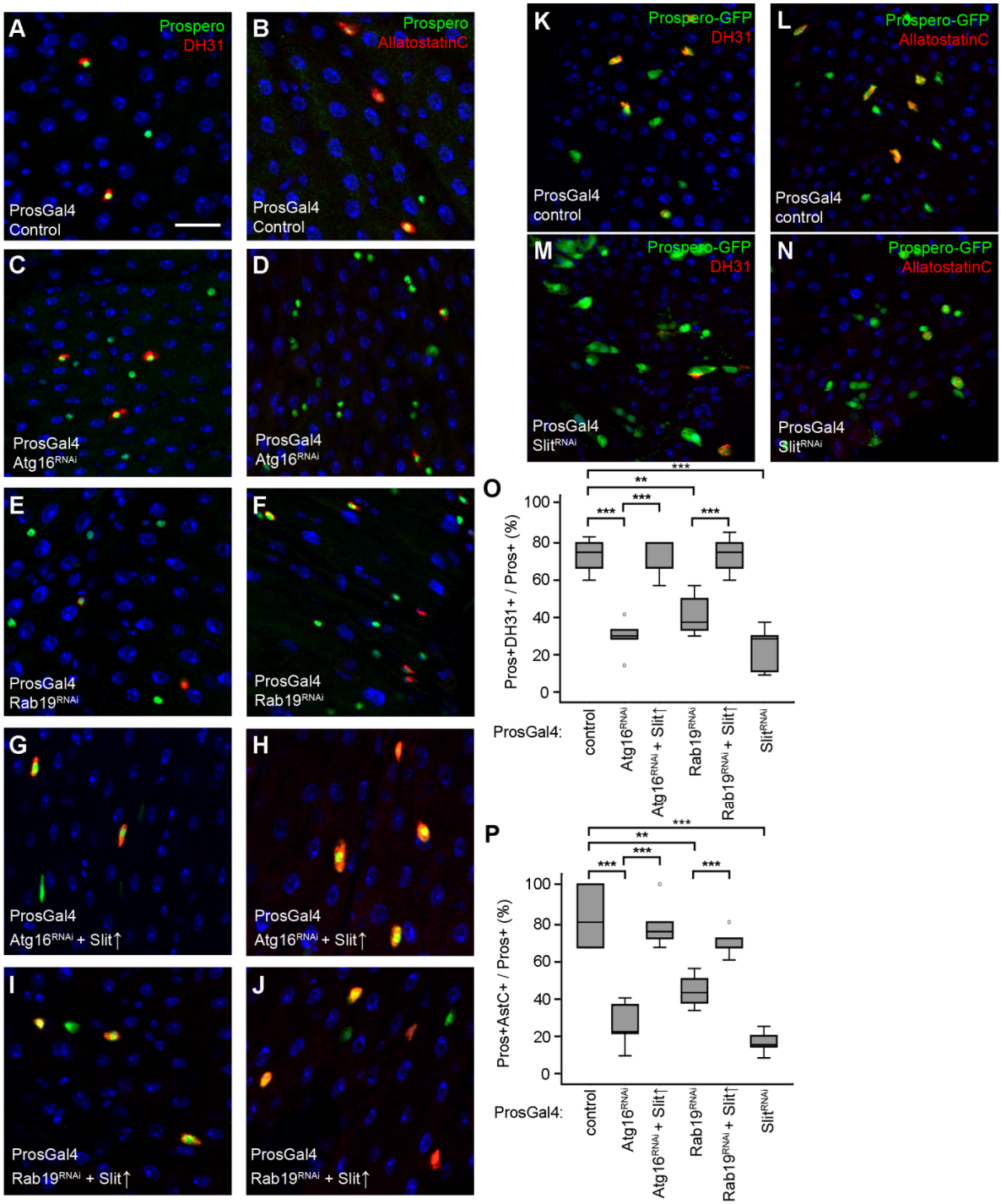

Fig. S10: EE lineage-specific knockdown of *Atg16* or *Rab19* perturbs peptide hormone secretion in a Slit-dependent manner

Expression of DH31 (A) and AllatostatinC (B) in control midguts. Prospero-specific *Atg16* (C, D) or *Rab19* (E, F) RNAi decreases the ratio of Prospero-positive cells

producing DH31 and AllatostatinC. (H). Overexpression of Slit (G-J) restores peptide hormone expression in *Atg16 (*G, H) and *Rab19* (I, J) RNAi cells. RNAi silencing of *slit* decreases the ratio of DH31-positive EE cells (M) compared to controls (K). Similarly, knockdown of *slit* decreases the ratio of AllatostatinC-positive EE cells (N) compared to controls (L). Prospero-positive cells were labeled by anti-Pros for A-J and by anti-GFP for K-N. Quantification of data from A, C, E, G, I, K, M (O) and B, D, F, H, J, L, N (P). The last quarter of the posterior midgut was sampled for DH31 and the first half of the posterior midgut was sampled for AstC, respectively, because we detected highest peptide expression in those subregions. N=5, ***: $p<0.001$, **: $p<0.01$, based on ANOVA for both O and P. Bar: 20 µm for A-N.

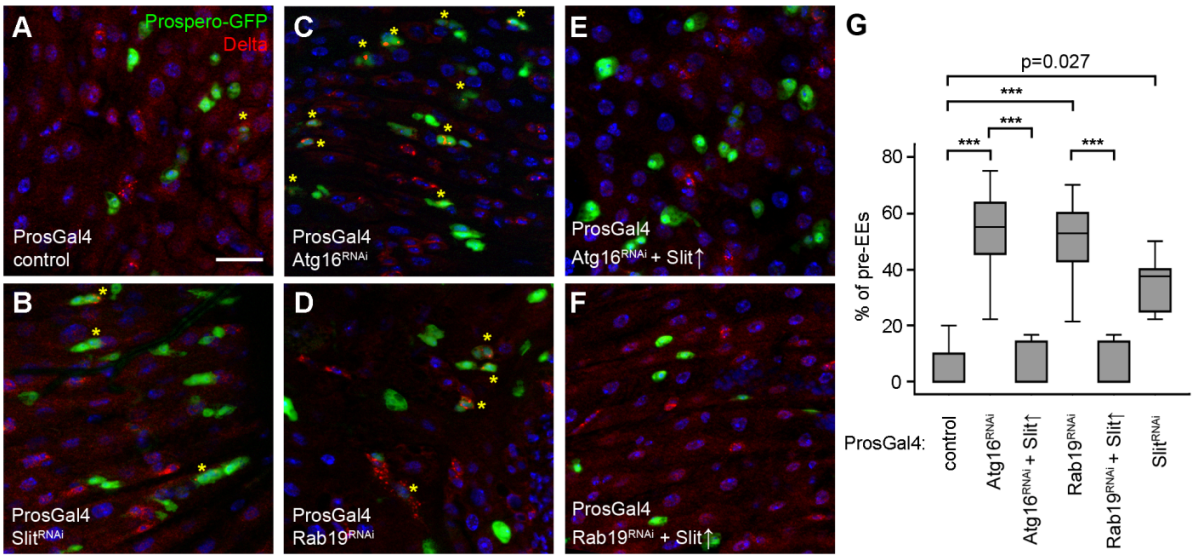

Fig. S11: EE lineage-specific knockdown of *Atg16* or *Rab19* perturbs EE differentiation in a Slit-dependent manner

Pre-EEs positive for both Prospero and Delta (asterisk) are rarely detected in control midguts (A). Prospero-specific knockdown of *slit* (B), *Atg16* (C) or *Rab19* (D) increases the ratio of pre-EEs containing both Prospero and Delta. Overexpression of Slit restores pre-EE cell number in Prospero-specific *Atg16* (E) and *Rab19* (F) RNAi guts. (G) Quantification of data. N=5, ***: p<0.001, Kruskal-Wallis test. Bar: 20 µm for A-F.